Performance of Larger-Volume 40 × 40 × 10- and 40 × 40 × 15-mm^3 CdZnTe Detectors

Yuefeng Zhu and Zhong He, *Senior Member, IEEE*

***Abstract*— The dimension of 20 × 20 × 15 mm^3 has been selected as standard pixelated CdZnTe detector size for many years. Energy resolution of 0.31% full-width at half-maximum (FWHM) at 662 keV for single-pixel events was achieved in one of the best direct-attachment detectors based on VAD_UM v2.2 application-specific integrated circuit (ASIC). Energy resolution under 0.40% was obtained for most of the direct-attachment detectors. The consistent good performance drives the desire to build larger crystals. The increment of size is beneficial in many aspects, such as higher detection efficiency, better imaging performance, better spectroscopic resolution, and potentially lower cost. This article presents the performance of recently delivered 40 × 40 × 10 and 40 × 40 × 15-mm^3 CdZnTe crystals manufactured by Redlen Technology and Kromek Group. The result will be analyzed and the feasibility of mass producing 40 × 40-mm^2 crystals will be discussed.**

***Index Terms*— CdZnTe, large volume, pixelated, semiconductor radiation detector.**

I. Introduction

As a room-temperature alternative to high purity germanium (HPGe), CdZnTe has been researched on for more than two decades. Pixelated design developed by University of Michigan was proved capable of achieving excellent spectroscopic performance. A decade ago, the resolution of pixelated CdZnTe crystals using VAS/TAT application-specific integrated circuits (ASICs) was about 0.70% full-width at half-maximum (FWHM) at 662 keV for single-pixel events [1]. After years of effort, direct-attachment CdZnTe detector modules using 1.5-keV noise VAD_UM v2.2 digital ASIC can achieve close to 0.30% FWHM [2], [3]. More important, most of the direct-attachment modules have energy resolution below 0.40% as plotted in Fig. 1. This consistent performance indicates the high yield of high-quality material. It motivates us to start the development of next-generation larger-volume CdZnTe detectors. Some work has been done for thick detectors up to 50 mm [4]. To us, larger lateral area is more interesting. The dimension 40 × 40 × 15 mm^3 is then picked for our next-generation CdZnTe detector size.

For many years, 20 × 20 × 15 mm^3 has been used as the standard dimensions for pixelated CdZnTe detectors at University of Michigan based on practical availability. If the size can be increased, for example, 40 × 40 × 15 mm^3, it can benefit in many aspects. First, the efficiency of the detector can be improved. To reduce the leakage on anode pixels, there is a guard ring surrounding the anode pixels. In the guard ring region, the volume is not fully active. Depending on the guard ring bias and detector surface properties, many events can be collected by the guard ring and become lost. Smaller guard ring region fraction is preferred to reduce inactive detection volume. A 2-×-2 20 × 20 × 15-mm^3 array and a single 40 × 40 × 15 mm^3 have the same physical volume. But the later one has smaller guard ring region and therefore higher efficiency. Second, for low-energy traditional coded-aperture imaging, larger crystals can provide better performance because of better uniformity across the detector detection area. A detector array always has gap between individual detectors. Events falling inside the gap will be lost. It causes artifacts in reconstructed coded-aperture images. There are several methods invented to deal with the problem. One example is time-encoded coded-aperture imaging [5]. It can completely remove artifact caused by the gap. However, it has very long scan time. As a result, for moving targets scenario, time-encoded method cannot be applied. A single 40 × 40 × 15-mm^3 detector provides continuous imaging area without any gap in the middle. Traditional coded-aperture techniques can be directly employed to optimize the performance with minimum development effort. Third, larger crystals are beneficial for spectroscopic performance. It is observed that the edge pixels usually have poorer energy resolution than inner pixels because of weighting potential deviation. Operating field distortion near detector edge can also complicate charge transportation and cause signal degradation. Larger crystals reduce the fraction of edge pixels. Therefore, the spectroscopic performance of larger crystals

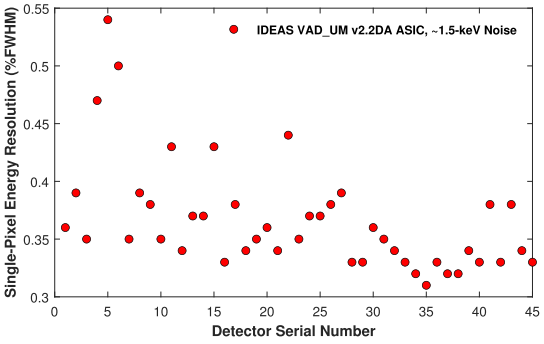

Fig. 1. Performance of Redlen direct-attachment detectors using VAD_UM v2.2 ASIC received in 2016 and 2017.

Manuscript received April 23, 2020; revised July 3, 2020; accepted January 12, 2021. Date of publication January 18, 2021; date of current version February 16, 2021. This work was supported by the Defense Threat Reduction Agency under Contract HDTRA1-18-C0073.

The authors are with the Department of Nuclear Engineering and Radiology Sciences, University of Michigan, Ann Arbor, MI 48109 USA (e-mail: zhuyuef@umich.edu).

Color versions of one or more figures in this article are available at https://doi.org/10.1109/TNS.2021.3052133.

Digital Object Identifier 10.1109/TNS.2021.3052133

can be better. Finally, the cost of one 40 × 40 × 15-mm^3 crystal could be lower than four 20 × 20 × 15-mm^3 crystals because of the saving of fabrication effort. The prerequisite is the high yield of high-quality crystals. The quality of CdZnTe material has been proved consistent in recent years. It implies the possibility to produce large 40 × 40 × 15-mm^3 crystals at similar yield as small 20 × 20 × 15-mm^3 crystals. Fabrication, such as attaching a crystal to its substrate, takes effort for each individual crystal no matter what the size the crystal is. Making multiple small detectors takes more fabrication effort than one single large detector intuitively. Because of this, the cost of one 40 × 40 × 15-mm^3 CdZnTe detector could be eventually less than four 20 × 20 × 15-mm^3 detectors combined, which will make 40 × 40 × 15-mm^3 crystals economically favorable. For practical applications, 24-cm^3 CdZnTe (volume of four 20 × 20 × 15 mm^3 or one 40 × 40 × 15 mm^3) can achieve similar detection efficiency as commonly used 2-in diameter NaI(Tl) cylinder detectors [6].

In 2018, two 40 × 40 × 15-mm^3 detectors ordered from the CdZnTe division of Kromek Group or formerly eV Product (Kromek/eV) were delivered. One of them was fully active and showed 0.83% FWHM energy resolution at 662 keV using 2-keV noise VAD_UM v2.2 ASIC modules. It demonstrated the possibility to fabricate such large crystals. In 2019, eleven large detectors were ordered and successfully delivered, including four 40 × 40 × 15-mm^3 and two 40 × 40 × 10-mm^3 crystals from Redlen Technologies and five 40 × 40 × 15-mm^3 crystals from Kromek/eV. For convenience, those detectors are called 40 × 40-mm^2 detectors for the rest of the article. The old smaller crystals are then called 20 × 20-mm^2 crystals. All the 40 × 40-mm^2 crystals are evaluated using the Brookhaven National Lab (BNL) H3D ASIC with 2.0-keV electronic noise. Their performance will be reported and analyzed.

II. Design and Readout of 40 × 40-mm^2 Crystals

The anode pixel of 40 × 40-mm^2 crystals has a slightly larger pitch than 20 × 20-mm^2 detectors because of the shrunk guard-ring area. Its pitch is 1.77 mm compared to 1.72 mm of smaller crystals. Similar small-pixel effect is expected. The cathode and guard ring are separated into four quadrants to reduce the capacitance and leakage. Each cathode and grid quadrant is connected to one ASIC during detector benchmark. It was discovered that when events happened close to the quadrant boundary, cathode signal induction would be distorted by cathode small-pixel effect. It is a potential problem. The details will be discussed in Section IV-B.

The total pixel number is 22 × 22 for 40 × 40-mm^2 detectors. To readout all 484 pixels, four BNL H3D ASIC [7] modules are used as shown in Fig. 2. Each ASIC is responsible for reading out one quadrant of the entire crystal. BNL H3D ASIC is an analog ASIC with about 2.0-keV electronic noise. It has 130 channels. Two of them are special channels for cathode and guard ring signals. The other 128 channels are for the pixel anode; 121 of them are connected to the 11 × 11 pixels and the other seven are left unused. With a good CdZnTe crystal plugged in, BNL H3D ASIC can give as good as 0.48% FWHM energy resolution at 662 keV for single-pixel events. The entire module is plugged into a 3 × 3 array readout system [7] and then route to a PC via the USB interface. Data acquired from the BNL H3D ASICs will be processed and calibrated on the PC. The array system is a prototype system and does not have appropriate cooling design. To avoid overheating and keep the detector at room temperature, a small Peltier-powered fridge is used. It houses the whole array system and provides enough cooling power to make the detector ambient stay round 20 °C–25 °C.

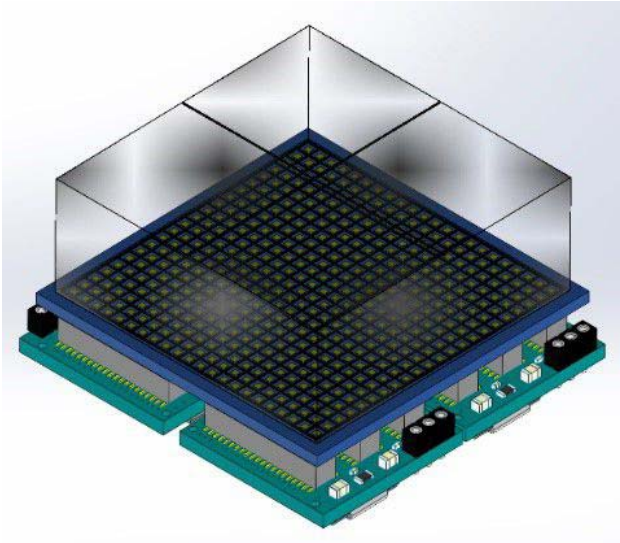

Fig. 2. Illustration of a 40 × 40-mm^2 detector and its readout mechanism.

III. Detector Performance

There are two important factors determining the detector performance: fabrication quality and material quality. For a large crystal with 40 × 40-mm^2 area, attaching the detector reliably to the substrate is a challenging task. Dead pixel and gain deficit are two major problems related to the fabrication process. Gain deficit is defined as amplitude reduction of gamma-ray-induced signals. It can be measured by the position of 662-keV photopeak centroid. A several-percent smaller photopeak centroid is usually observed in gain-deficit pixels than in normal pixels. It naturally makes the signal-to-noise ratio smaller. In addition, the gain of gain-deficit pixels can change in a random and abrupt manner as a function of operation duration and ambient temperature. This feature makes gain-deficit pixels unreliable in practical applications.

When attachment is completely failed and the detector is broken from the substrate, no signal can be passed to the ASIC and the pixel is dead. When attachment is not fully failed, extra resistance or capacitance or both might be created between the detector pixel and the substrate. In this case, induced signal will not be fully collected by the collecting pixel preamp. A fraction of it could be lost to the neighbor pixels. This is believed to be one of the major causes of the gain-deficit problem. Recently, we discovered that using annealing, gain deficit can be improved [8]. It is likely because thermal expansion fixed the attachment defects.

Table I summarizes fabrication problems found in the eleven 40 × 40-mm^2 detectors. 8R and 9R series detectors are

TABLE I
SUMMARY OF DEAD PIXELS AND GAIN-DEFICIT PROBLEMS

Detector Serial #	Dead Pixels	Gain-deficit Pixels
8R1	2	0
8R2	4	1
9R1	4	5
9R2	4	3
9R3	1	0
9R4	11	3
9E1	3	237
9E2	0	225
9E3	0	176
9E4	1	198
9E5	0	156

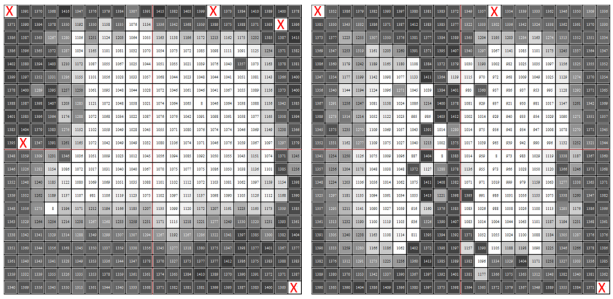

Fig. 3. Illustration of the gain-deficit problem found in the Kromek/eV 9E detectors. The color scale represents the photopeak amplitude of the 662-keV spectra collected in each pixel. The range is from 1100 to 1500 analog to digital converter (ADC).

$40 \times 40 \times 10$ and $40 \times 40 \times 15$-mm^3 crystals from Redlen. 9E series detectors are $40 \times 40 \times 15$-mm^3 crystals made by Kromek/eV. The two 10-mm-thick 8R detectors have excellent fabrication quality. There is almost no gain-deficit problem found and the number of dead pixels is small. The four 15-mm-thick 9R detectors have similar fabrication quality as 8R detectors. Most of them have very small number of gain-deficit and dead pixels. Detector 9R4 has the worst fabrication quality but still acceptable. As for Kromek/eV detectors, the number of dead pixels is negligible. However, there are significant amount of gain-deficit pixels. Fig. 3 presents the location map of the gain-deficit pixels. Each square represents one anode pixel. The color scale gives the photopeak amplitude of the 662-keV spectra. The crossed pixels are connected to damaged ASIC channels and they should be ignored in our discussion. The white pixels have the gain-deficit problem. The left plot is observed in detector 9E1 and the right is for detector 9E2. Those are two typical gain-deficit patterns. It indicates that the surface of the crystal might not be polished flat enough. For such large 40×40-mm^2 area, it is expected that surface polishing process is a significant challenge.

Material quality is benchmarked by energy resolution and electron trapping or the $\mu\tau$ product. The overall performance of 40×40-mm^2 detectors is presented in Fig. 4. Electrons' $\mu\tau$ product is calculated using the method described in [11]. The energy spectra of the 662-keV ^{137}Cs source for three best crystals is shown in Fig. 5. The spectra is from all single-pixel events in the entire 40×40-mm^2 detector volume. Most Redlen detectors achieved better than 0.60% FWHM energy resolution at 662 keV for single-pixel events. Three of five Kromek/eV detectors have about 0.70% energy resolution.

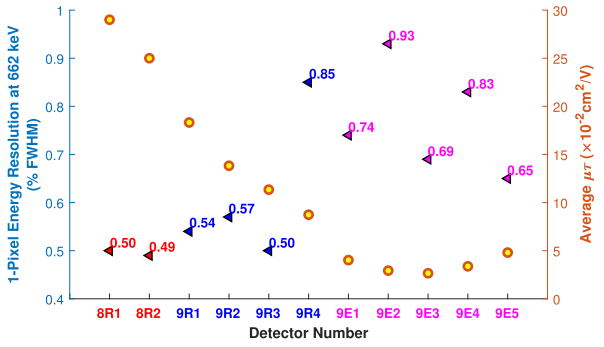

Fig. 4. Single-pixel events energy resolution and average electron $\mu\tau$ product of the 40×40-mm^2 detectors. The triangle markers give energy resolution at 662 keV and number on top of the marker is the resolution value in percentage FWHM. The circle represents electron's average $\mu\tau$ product of the whole detector.

In practice, it is usually required to have 1% energy resolution at 662 keV for all events, which is about 0.7% FWHM for single-pixel events. Therefore, for these eleven 40×40-mm^2 detectors, eight detectors passed the 1% FWHM requirement. The yield is about 70%, which is encouraging.

Electron's $\mu\tau$ product for both Redlen and Kromek/eV detectors is high. Redlen detectors have less trapping than Kromek/eV detectors. Several of Redlen detectors can even reach 10^{-1} cm^2/V electron $\mu\tau$. However, the correlation between electron trapping and energy resolution is vague. Fig. 6 plots the the channel-by-channel correlation between electrons' $\mu\tau$ product and energy resolution for the 9R and 9E detectors. Many channels have similar trapping but diverse energy resolution. For example, most channels in detectors 9E4 and 9E5 are located at the same region along the $\mu\tau$ axis but their energy resolution distribution is significantly different. Generally speaking, statistical fluctuation of trapping is negligible for high $\mu\tau$ detectors, such as those above 10^{-2} cm^2/V. Material nonuniformity or trapping variation inside the detector is a more important factor. The cause of poorer energy resolution in Kromek/eV detectors could be due to more severe material nonuniformity. However, in Section IV-A, more detailed study is carried out and a more possible cause is revealed.

IV. ANALYSIS AND DISCUSSION

A. Material Quality

Three-dimensional position sensing is a powerful tool to look into the details of the material quality. It can break a measurement into a distribution on small voxels to help people understand the characteristics of the measurement and related detector properties. In pixelated detectors, 3-D position sensing is achieved based on signal induction difference between cathode and anode electrodes [9]. The lateral location is naturally obtained by location of the triggered pixel. The interaction depth can be obtained by two methods: C/A ratio or drift time. The C/A ratio is the ratio between cathode and anode signal amplitudes. For single-polarity charge sensing, it is an effective way to obtain interaction depth for single-pixel-triggered events or single-pixel events. According to Schokley–Ramo theory, signal induced on a planar electrode

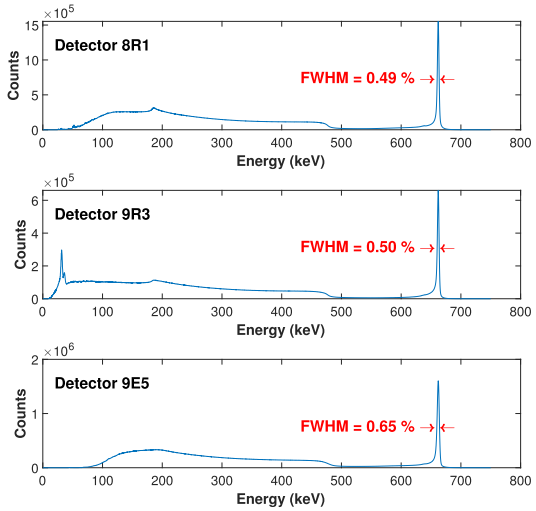

Fig. 5. Single-pixel events spectra of the entire 40 × 40-mm^2 detector volume for the best crystals among 8R, 9R, and 9E series detectors. The source is ^{137}Cs illuminating from the cathode side.

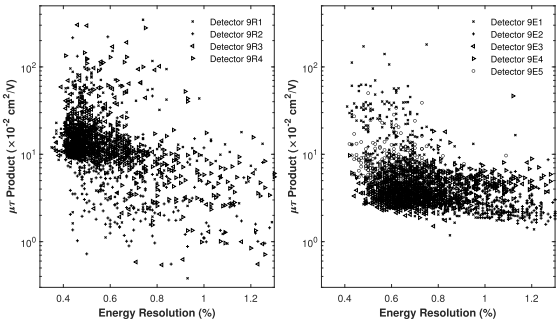

Fig. 6. Single-pixel events energy resolution versus electron's $\mu\tau$ product for each pixel in the 9R and 9E detectors.

is proportional to the depth of the carrier, while signal induced on a pixel anode is almost constant unless the interaction is close to the pixels. It is called small-pixel effect. In CdZnTe detectors, electrons are the major carriers since holes move ten times slower than electrons and they are much easier to get trapped. The ratio between signals induced on the planar cathode and the pixelated anode is a linear function of depth and depth only. The linearity breaks only when the interaction happens next to the anode surface. Drift time is another way to obtain depth information. Signal induced on a planar electrode rises immediately after the interaction happens, while signal induced on a pixel is negligible until the charge reaches the vicinity of the pixel. In CdZnTe detectors, cathode signal start time can be used to mark the start of the electron drift and the anode signal rising gives the end time. The C/A ratio and drift time have different advantages and problems. The C/A ratio has very high depth resolution and it is independent of operating conditions (such as cathode bias) and material properties (such as nonuniformity). However, the C/A ratio cannot work for multiple-pixel-triggered events or multipixel events. When multipixel events happen, the cathode signal could be the sum of the induced signals from several electron clouds. The C/A ratio will not be a simple function of individual depth. Then drift time becomes the only way to tell the interaction depth of the electron clouds under each pixel.

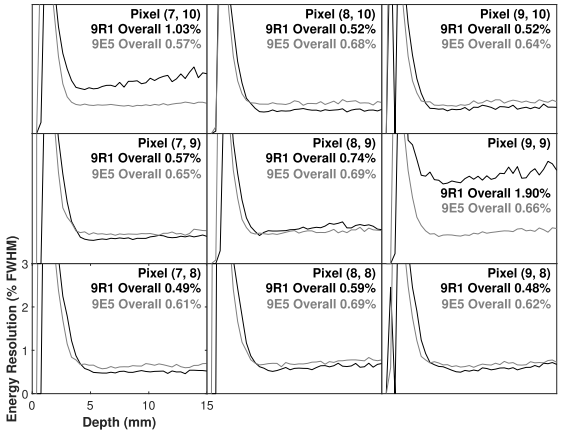

Fig. 7. Single-pixel energy resolution as a function of depth for the pixels located from (7, 8) to (9, 10) in detectors 9R1 and 9E5. Depth 0 mm is anode side, while depth 15 mm is cathode side. Black lines are for detector 9R1, while gray lines are for detector 9E5.

Rich information can be revealed via the plot of measurements as a function of 3-D position. Fig. 7 gives an example of single-pixel energy resolution as a function of depth for those pixels located from coordinates (7, 8) to (9, 10) in Redlen detector 9R1 and Kromek/eV detector 9E5. The coordinate is defined from (1, 1) to (22, 22). The region is chosen because it contains several typical types of observations.

Fig. 7 presents the data from the two detectors. Let us focus on detector 9R1 first, which is presented by the black curves. In this detector, pixel (8, 10) is a good pixel with overall resolution at 0.52%. In the bulk region, its energy resolution is not sensitive to depth. The degradation of energy resolution close to the anode side is due to rapid variation of weighting potential along both depth and lateral direction. As a comparison, pixel (7, 10) has a strong degradation toward cathode side. Such observation indicates more trapping which causes poorer resolution in this pixel. For pixel (8, 10), since the curve is flat in the bulk region, electronic noise is believed to be the major contributor. In fact, the measured noise of pixel (8, 10) in detector 9R1 is 2.3 keV or 0.35% FWHM with −3000 V cathode bias. The statistic uncertainty of 662-keV energy deposition is about 0.21% FWHM considering the Fano factor to be 0.1. These two uncertainties are not a function of depth and they add up to be 0.41%. It dominates the observed 0.52% total photopeak FWHM. Therefore, a flat resolution curve as a function of depth is expected. Among other pixels in detector 9R1, pixel (8, 9) also has resolution degradation toward cathode side but less severe than pixel (7, 10). Therefore, it has poorer overall resolution than pixel (8,10) but better than (7, 10). Pixel (9, 9) does not show clear resolution degradation toward cathode. It has poor resolution over all depth. This is due to high electronic noise, which is measured to be 11.1 keV at −3000 V cathode bias. As we know, leakage current under each pixel varies. Pixel (9, 9) might have very large leakage due to some crystal defects and the leakage causes the large amount of parallel noise.

As for Kromek/eV detector 9E5, it is observed that there are many pixels with flat curves in bulk region with energy resolution uniformly worse than Redlen detector 9R1.

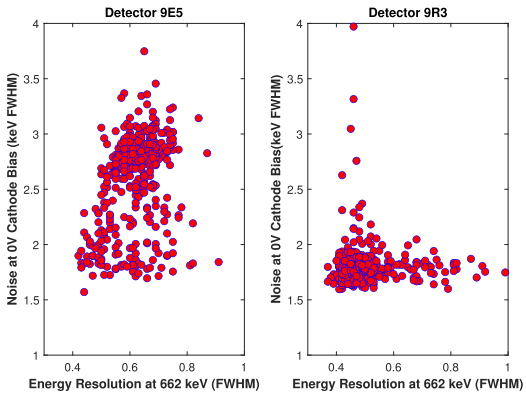

Fig. 8. Plot of single-pixel energy resolution at 662 keV versus electronic noise with 0-V cathode bias for all 484 pixels in detectors 9E5 and 9R3. Electronic noise is obtained using test pulse.

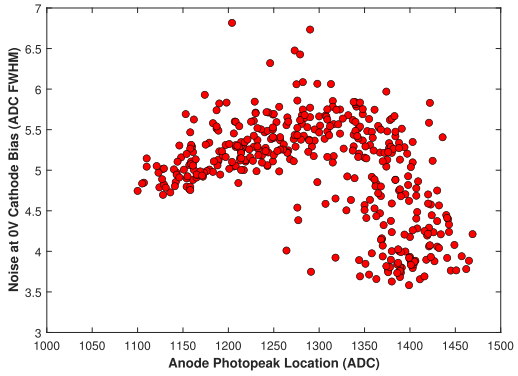

Fig. 9. Correlation between gain deficit and electronic noise measured at 0 V for detector 9E5.

TABLE II

SUMMARY OF THE QUALITY OF 40 × 40-mm^2 DETECTORS. THE LEAKAGE IS TAKEN AT −3000 V CATHODE BIAS UNLESS SPECIFIED

Detector Serial #	Energy Resolution (%)	Leakage (nA)	Poor Trapping Pixels (%)
8R1	0.50	243@2kV	3.93
8R2	0.49	224@2.5kV	1.45
9R1	0.54	475	14.46
9R2	0.57	321	26.65
9R3	0.50	253	8.26
9R4	0.85	407	43.60
9E1	0.74	135	39.67
9E2	0.93	201	48.35
9E3	0.69	258	18.39
9E4	0.83	190	27.89
9E5	0.65	131	2.69

According to the discussion above, it implies that detector 9E5 has higher electronic noise than those on detector 9R1. The energy resolution of detector 9E5 must be dominated by electronic noise. Fig. 8 plots measured electronic noise versus energy resolution for all 484 pixels on detectors 9E5 and 9R3. In the plot for detector 9E5, energy resolution has clear correlation with electronic noise. Most of the pixels in detector 9E5 have high noise and then their energy resolution is poor and more than 0.6%. But some pixels have small electronic noise and then their energy resolution is as good as 0.5%. Comparing with the plot for Redlen detector 9R3, one can find that with low electronic noise, both 9E5 and 9R3 can achieve energy resolution around 0.5%. This observation indicates that the performance of the detector 9E5 is limited by electronic noise instead of material quality. Electronic noise is a function of both leakage and input capacitance. As shown in Table II, leakage is apparently not the limiting factor on Kromek/eV detectors since Redlen detectors have much larger leakage but performs much better than Kromek/eV detectors. Therefore, input capacitance must be the dominating factor causing degraded performance in Kromek/eV's 40 × 40-mm^2 detectors.

In past years, it has been found that the input capacitance is correlated with several factors, including trace length from the pixel anode to the input of the ASIC preamplifier [2], impedance between neighboring pixels, size of the anode pixels, and so on. After careful examination, it was discovered that the fabrication flaw that leads to gain deficit in the Kromek/eV detectors is likely the cause. A strong correlation was discovered between gain deficit and electronic noise, as shown in Fig. 9. All the gain-deficit pixels were found noisier at 0-V cathode bias than normal pixels, indicating that extra input capacitance was added with flawed fabrication.

Based on the above discussion, one can determine material quality by investigating the number of pixels with degrading resolution along depth. Detectors with different electronic noise can be compared in this way to find out the quality of the material. Table II summarizes the fraction of those "poor-trapping" pixels in each 40 × 40-mm^2 detectors. Although detector 9E5 has poorer energy resolution than Redlen detectors, it seems to have high-quality material similar to the best Redlen detector 9R3. Detectors 9E3 and 9E4 have poorer material but they are similar to Redlen detectors 9R1 and 9R2. This result indicates that Kromek/eV might be able to produce CdZnTe crystals similar to Redlen detectors.

B. Cathode Signal Distortion

In our 40 × 40-mm^2 detectors, the cathode is divided into four quadrants. There are two reasons to do so. First, four cathode quadrants are placed to reduce the risk of severe material problems. If a single planar cathode is made for 40 × 40-mm^2 detectors, the cathode will see four times larger leakage and capacitance comparing to the old 20 × 20-mm^2 detectors. Cathode preamp might not be able to handle such change and it can cause significant increment of noise. Second, our electronics has limitations. The ASICs available in our laboratory, including Ideas VAD_UM ASIC and BNL H3D ASIC, were designed to trigger from anode pixels instead of cathode to reduce noisy triggering. However, this triggering mechanism becomes a problem when multiple ASICs are used to readout a single detector. If a single cathode is present, the cathode can only be connected to one ASIC. When events happen on the pixels in other ASICs, the cathode-connected ASIC will not have any trigger and the cathode signal will be lost. There is an option that one can connect the single cathode to all the four ASICs simultaneously. However, the signal amplitude will then drop about four times and the noise will increase at least two times. The signal-to-noise ratio will significantly degrade. For those 40 × 40-mm^2 detectors, four ASICs are used to read out the 484 pixels. This readout scheme makes it incompatible with the single-cathode design. The best solution is to develop an ASIC with interchip

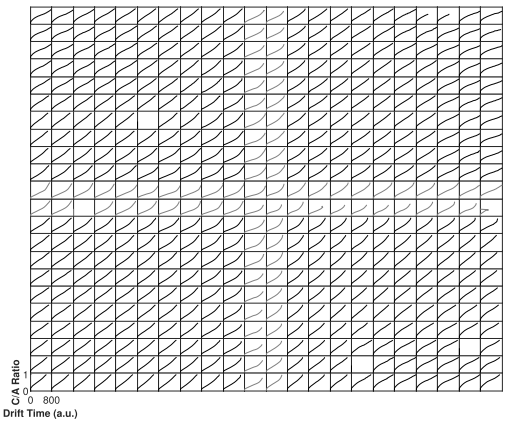

Fig. 10. C/A ratio as a function of drift time for each pixel in detector 9R2. The gray lines are those pixels along the quadrant boundary.

triggering capability. Any trigger generated in one ASIC can be passed to the cathode-connected ASIC for cathode signal readout. This new generation of ASIC is under development.

The four-cathode-quadrant design can work perfectly for energy reconstruction of single-pixel events. However, it becomes a problem for depth reconstruction and multipixel events reconstruction. When an event happens close to the boundary of the quadrants, cathode weighting potential will be affected by small-(cathode)-pixel effect and no longer a linear function of the depth. Fig. 10 plots the C/A ratio as a function of drift time for detector 9R2. As we know, for an ideal detector, both the drift time and C/A ratio are linear functions of depth and their relative relationship is also a linear function. Inside each quadrant, it can be observed that the drift time is approximately linear to the C/A ratio as one expects. However, for the pixels close to the quadrant boundary, the linearity no longer keeps. Such curvature along the quadrant boundary is due to cathode weighting potential nonlinearity.

The cathode weighting potential nonlinearity depends on the distance between the interaction and the quadrant boundary. As depicted in Fig. 10, the curvature gets more and more severe when the pixel location is closer and closer to the boundary. It makes it difficult to calibrate the C/A ratio and calculate the real interaction depth for those pixels. For a linear relationship, the boundary of the C/A ratio depth distribution is sufficient to calibrate. However, for a nonlinear relationship, collimation measurement is required. As for multipixel events, the calibration of energy and depth is difficult for nonlinear cathode weighting potential. To make the calibration time and data size reasonable, multipixel reconstruction assumes that the crosstalk is similar for all pixels if their depth is the same [10]. This assumption is apparently invalid for the quadrant boundary pixels. One can rely on simulation to predict the cathode weighting potential nonlinearity or use drift time to calculate depth. However, simulation usually cannot duplicate many practical parameters such as trapping, electrode fabrication, defects, space charge, and so on. And the drift time is sensitive to material properties such as uniformity, bias voltage, temperature, and so on. Both of them can work in theory but is very difficult to implement in practical applications. A single cathode is so far the best way to operate such a large crystal.

V. Conclusion

In this article, the performance of eleven 40 × 40-mm^2 detectors are reported. The single-pixel energy resolution of eight of them are found below or around 0.7% FWHM at 662 keV using BNL H3D analog ASIC. For all events combined, it is expected that these eight detectors can achieve 1% FWHM energy resolution. It is a promising result to show that high-quality large-volume 40 × 40-mm^2 detectors are feasible to manufacture with reasonable yield. A fabrication problem is identified for Kromek/eV detectors, which causes severe gain-deficit problem in the center of the detector. However, the material quality of Kromek/eV detectors is found acceptable. Several Kromek/eV detectors' material quality is close to Redlen's material, although the measured energy resolution of detectors is much poorer. The cause is found due to high electronic noise from excessive input capacitance.

In general, 40 × 40-mm^2 detectors have been proved to be a feasible option for practical applications. The benefits of the larger crystals can help further improve the performance of CdZnTe detectors.

Acknowledgment

Any opinions, findings, and conclusions or recommendations expressed in this material are those of the author(s) and do not necessarily reflect the views of the Defense Threat Reduction Agency.

References

[1] F. Zhang, Z. He, G. F. Knoll, D. K. Wehe, and J. E. Berry, "3-D position sensitive CdZnTe spectrometer performance using third generation VAS/TAT readout electronics," *IEEE Trans. Nucl. Sci.*, vol. 52, no. 5, pp. 2009–2016, Oct. 2005.

[2] M. Streicher, S. Brown, Y. Zhu, D. Goodman, and Z. He, "Special nuclear material characterization using digital 3-D position sensitive CdZnTe detectors and high purity germanium spectrometers," *IEEE Trans. Nucl. Sci.*, vol. 63, no. 5, pp. 2649–2656, 2016.

[3] Y. Zhu and Z. He, "Performance of a 2-keV digitizer ASIC for 3-D position-sensitive pixellated semiconductor detectors," in *Proc. IEEE Nuclear Nucl. Sci. Symp. Conf.*, Oct./Nov. 2012, pp. 4109–4112.

[4] A. E. Bolotnikov *et al.*, "CdZnTe position-sensitive drift detectors with thicknesses up to 5 cm," *Appl. Phys. Lett.*, vol. 108, no. 9, Feb. 2016, Art. no. 093504.

[5] S. Brown, "Time-encoded thermal neutron imaging using large-volume pixelated CdZnTe detectors," Ph.D. dissertation, Dept. Nucl. Eng. Radiol. Sci., Univ. Michigan, Ann Arbor, MI, USA, 2017.

[6] M. Streicher, "Applications of digitized 3-D position-sensitive CdZnTe spectrometers for national security and nuclear nonproliferation," Ph.D. dissertation, Dept. Nucl. Eng. Radiol. Sci., Univ. Michigan, Ann Arbor, MI, USA, 2017.

[7] F. Zhang, C. Herman, Z. He, G. D. Geronimo, E. Vernon, and J. Fried, "Characterization of the H3D ASIC readout system and 6.0 cm^3 3-D position sensitive CdZnTe detectors," *IEEE Trans. Nucl. Sci.*, vol. 59, no. 1, pp. 236–242, Feb. 2012.

[8] J. Xia, "Interaction reconstruction in digital 3-D CdZnTe under various circumstances," Ph.D. dissertation, Dept. Nucl. Eng. Radiol. Sci., Univ. Michigan, Ann Arbor, MI, USA, 2019.

[9] Z. He, W. Li, G. F. Knoll, D. K. Wehe, J. Berry, and C. M. Stahle, "3-D position sensitive CdZnTe gamma-ray spectrometers," *Nucl. Instrum. Meth. Phys. Res. A, Accel., Spectrometers, Detectors Associated Equip.*, vol. 422, nos. 1–3, pp. 173–178, 1999.

[10] F. Zhang, "Events reconstruction in 3-D position sensitive CdZnTe gamma-ray spectrometers," Ph.D. dissertation, Dept. Nucl. Eng. Radiol. Sci., Univ. Michigan, Ann Arbor, MI, USA, 2005.

[11] Y. Boucher, F. Zhang, W. Kaye, and Z. He, "New measurement technique for the product of the electron mobility and mean free drift time for pixelated semiconductor detectors," *Nucl. Instrum. Meth. Phys. Res. A, Accel., Spectrometers, Detectors Associated Equip.*, vol. 671, no. 1, pp. 1–5, Apr. 2012.